J. Opt. A: Pure Appl. Opt. 1 (1999) 201–209. Printed in the UK PII: S1464-4258(99)97244-6

Earth–satellite–Earth laser long-path absorption experiment using the Retroreflector in Space (RIS) on the Advanced Earth Observing Satellite (ADEOS)

Nobuo Sugimoto†, Nobuhiko Koga†, Ichiro Matsui†, Yasuhiro Sasano†, Atsushi Minato‡, Kenichi Ozawa§, Yasunori Saito§, Akio Nomura§, Tetsuo Aoki‖, Toshikazu Itabe‖, Hiroo Kunimori‖, Isao Murata¶ and Hiroshi Fukunishi¶

† National Institute for Environmental Studies, 16-2 Onogawa, Tsukuba, Ibaraki 305, Japan
‡ Ibaraki University, 4-12-1, Naka-Narusawa, Hitachi 316, Japan
§ Shinshu University, 500 Wakasato, Nagano 380, Japan
‖ Communications Research Laboratory, 4-2-1 Nukui-kita, Koganei, Tokyo 184, Japan
¶ Tohoku University, Sendai 980, Japan

Received 7 September 1998, in final form 29 December 1998

Abstract. This paper reports the results of the laser long-path absorption experiments carried out with the Retroreflector in Space (RIS) on the Advanced Earth Observing Satellite (ADEOS). The RIS is a 0.5 m diameter single-element hollow retroreflector with a unique optical design which uses a curved mirror surface to correct velocity aberrations caused by the satellite movement. In the RIS experiments a laser beam was transmitted from a ground station, reflected by the RIS, and received back at the ground station. The absorption of the intervening atmosphere was measured in the round-trip optical path. After the launch of the ADEOS in August 1996, the optical characteristics of the RIS were tested, and it was confirmed that the RIS worked well in orbit. The spectroscopic measurement was carried out with the single-longitudinal-mode TEA CO_2 lasers by means of the method utilizing the Doppler shift of the reflected beam caused by the movement of the satellite. The spectrum of ozone was successfully measured in the 10 μm region, and the measurement of the column contents of ozone was validated with the simultaneous heterodyne spectrometer measurement. In June 1997, however, the experiment with the RIS was discontinued due to the malfunction of the ADEOS solar paddle.

Keywords: Satellite retroreflector, cube-corner retroreflector, laser long-path absorption method, carbon dioxide laser

1. Introduction

The laser long-path absorption method between the ground and a satellite is one of the most sensitive remote sensing techniques for measuring concentration of atmospheric trace species. Although global coverage is not obtained with this method, it can play a unique role in the measurement of trace species, especially in the troposphere where passive satellite sensors are not necessarily useful. The idea of the measurement using a satellite retroreflector was described in the paper by Hinkley (1976), although an experiment on this technique had not been implemented. The first experiment on Earth–satellite–Earth laser long-path absorption technique was carried out with the Retroreflector in Space (RIS) on the Advanced Earth Observing Satellite (ADEOS) which was launched by the National Space Development Agency of Japan (NASDA) in August 1996.

To perform Earth–satellite–Earth laser long-path absorption measurements, a large aperture retroreflector was required to obtain sufficient received power. It had to be a single-element retroreflector, because interference between elements in a retroreflector array would cause speckle noise in the spectrum measurements. Also, a method for optimizing the reflected beam pattern was required to correct velocity aberration caused by the satellite movement. The RIS was a 0.5 m diameter single-element hollow cube-corner retroreflector newly designed for the experiment. It had a unique design using a spherical mirror to optimize the reflected beam pattern.

1464-4258/99/020201+09$19.50

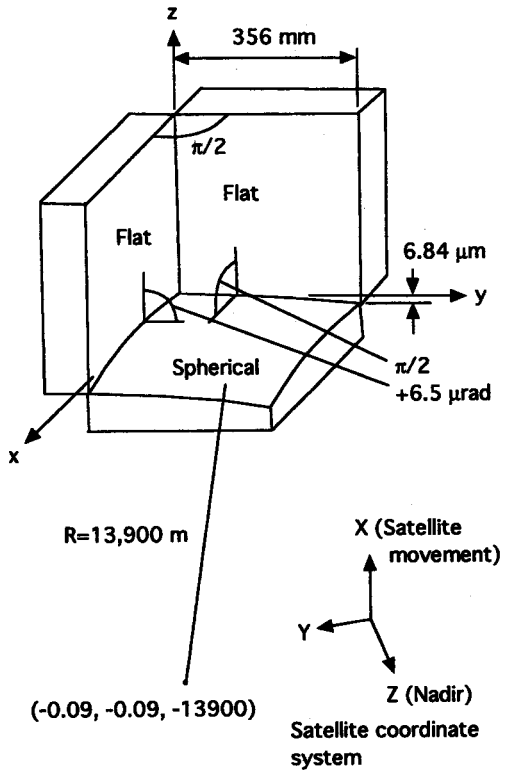

Figure 1. Surface structure of the RIS.

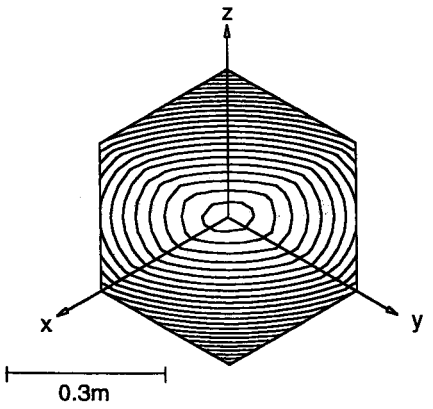

Figure 2. Simulated interference fringe of the RIS at 632 nm.

In the spectroscopic measurements, narrow-band pulsed tunable lasers were required. Two single-longitudinal-mode transverse, electric, atmospheric (TEA) CO_2 lasers were employed for the differential absorption spectroscopy measurement using the RIS. Since the CO_2 lasers are not continuously tunable, we developed a spectroscopic measurement method which utilized the Doppler shift of the reflected beam caused by the satellite movement. We originally planned the measurements of ozone, CFC12, HNO_3 with the fundamental of the CO_2 lasers, CO and N_2O with the second harmonics, and CH_4 with the third harmonics (Sugimoto *et al* 1995a).

After the successful launch of the ADEOS, we established the active tracking of the RIS using an image of the RIS lit by the second harmonics Nd:YAG laser at 532 nm. We then evaluated the optical characteristics of the RIS in orbit. After these initial experiments, we started experiments using the TEA CO_2 lasers. We carried out the measurement of ozone successfully using the Doppler shift method. We investigated measurement errors, and improved the transmitter/receiver system based on the investigation. The operation of the ADEOS, however, was discontinued by NASDA on June 30, 1997 due to the serious malfunction of the solar paddle. The experiment with the RIS was consequently discontinued. Although we were not able to implement the measurement experiments except for ozone, we obtained useful data for evaluating the measurement technique. This paper reports the results of the validation experiments of the measurement method using the RIS. In section 2, we describe the RIS on the ADEOS and the ground system for the long-path absorption experiments. In section 3, we report the optical characteristics of the RIS in orbit. We report the results of the spectroscopic measurement and error analysis in section 4.

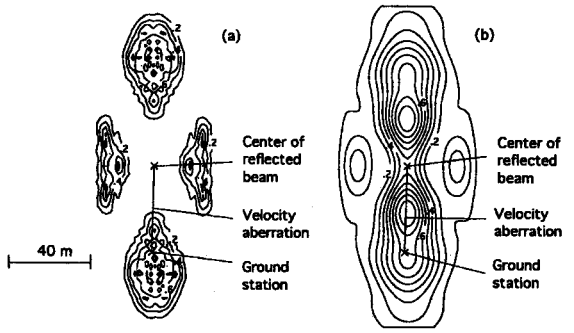

Figure 3. Ground patterns of the reflected beam intensity at (*a*) 532 nm and (*b*) 10 μm.

2. RIS on the ADEOS and the ground system

2.1. Design of the RIS

The RIS is a hollow cube-corner retroreflector having a spherical mirror to control the pattern of the reflected beam. We determined the surface parameters of the RIS with a computer simulation so that sufficient received power was obtained in a wide angular range. Figure 1 shows the surface structure of the RIS (Minato *et al* 1992). A spherical surface was used for the z surface along with 'spoiled angles' which are slightly changed from right angles. The radius of curvature of the z surface was approximately 14 km. Figure 2 shows the simulated wavefront of the reflected beam of the RIS when observed from the direction of the optical axis. The calculation was based on the ray tracing method. The ground pattern of the reflected beam was calculated from the simulated wavefront at the RIS by using Kirchhoff's equation for propagation of electromagnetic waves. Figures 3(*a*) and (*b*) show the ground patterns of the reflected beam intensity at 532 nm and 10 μm for the case where the transmitted beam is along the optical axis. The effect of the velocity aberration caused by the satellite movement was taken into account in

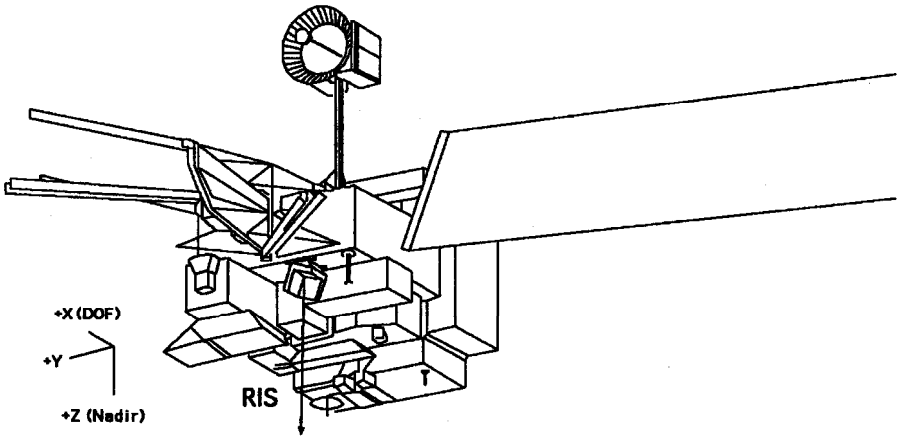

Figure 4. Geometry of the RIS on the ADEOS.

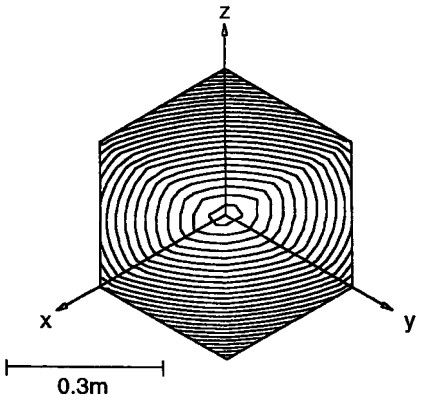

Figure 5. Estimated zero-gravity interferogram of the RIS PFM.

the simulation by shifting the reflected beam direction. The reflected beam is split along the satellite movement by the effect of the spoiled angles. The divergence of the reflected beam was determined by the effect of the spherical mirror at 532 nm. The divergence due to diffraction is comparable to the effect of the spherical mirror at 10 μm. In the design of the RIS, we optimized the spoiled angle and the curvature of the spherical mirror so that one of the split beams is received at the ground station efficiently.

The geometry of the RIS on the ADEOS is illustrated in figure 4. The mirror panels of the RIS were made of quartz with a light weighted structure developed by PLX Inc. (New York). The surface was finished with a silver-based optical coating. The housing was made of aluminum. The RIS was installed on the ADEOS so that the optical axis is directed to the ground with an angle of 30° toward the direction of the satellite movement from nadir. The ADEOS was a polar orbit satellite with an inclination of 98.6° and an altitude of 797 km. The RIS was used from a ground station when the RIS passed over one of the ground tracks within several hundred kilometres of the ground station and when the elevation angle was within the range of 30–90°.

We tested the RIS proto-flight model (PFM) with a 60 cm Zygo interferometer previously installed on the ADEOS. It was necessary to consider the effect of sag due to gravity in the measurement of the interferograms. In the test of the RIS PFM, we took interferograms at six rotational positions with the corner cube mounted horizontally. We calculated dihedral angles for the six interferograms and estimated the zero-gravity dihedral angles by taking the mean values (Sugimoto and Hinato 1994, Minato *et al* 1995). Figure 5 shows the estimated zero-gravity interferogram of the RIS PFM. It agreed well with the designed interferogram shown in figure 2.

2.2. Ground system for the RIS experiment

The ground system consists of an optical satellite tracking system and lasers for the spectroscopic measurement. We used the tracking telescope with a 1.5 m diameter at the Communications Research Laboratory in Koganei, Tokyo. A second-harmonics Nd:YAG laser performed active tracking by using the reflection image of the RIS, and was used for laser ranging to the ADEOS. The active tracking was performed concurrently with the programmed tracking to correct bias in programmed tracking. Two single-longitudinal-mode TEA CO_2 lasers were employed in the spectroscopic measurement (Nordstrom *et al* 1993, 1994). One of the lasers was used to measure the absorption of the target molecule, and the other to measure the reference signals to correct for atmospheric effects and the angular dependence of the RIS reflection.

We used the Doppler shift of a reflected beam caused by the satellite movement in the spectrum measurement with the RIS experiment (Sugimoto 1991, 1995b). Since the magnitude of the Doppler shift depends on the elevation angle to the ADEOS, the absorption spectra of the atmosphere can be measured using the change in the wavelength of the return beam. The Doppler shift can be expressed by

$$\Delta f = (2vf_0/c)\cos\theta, \tag{1}$$

where v is the velocity of the satellite, f_0 is the frequency of the laser, and θ is the elevation angle to the satellite. Since the speed of the ADEOS is 7 km s^{-1}, the spectral range covered by the Doppler shift is 0–1.3 GHz (0–0.04 cm^{-1}) at 10 μm.

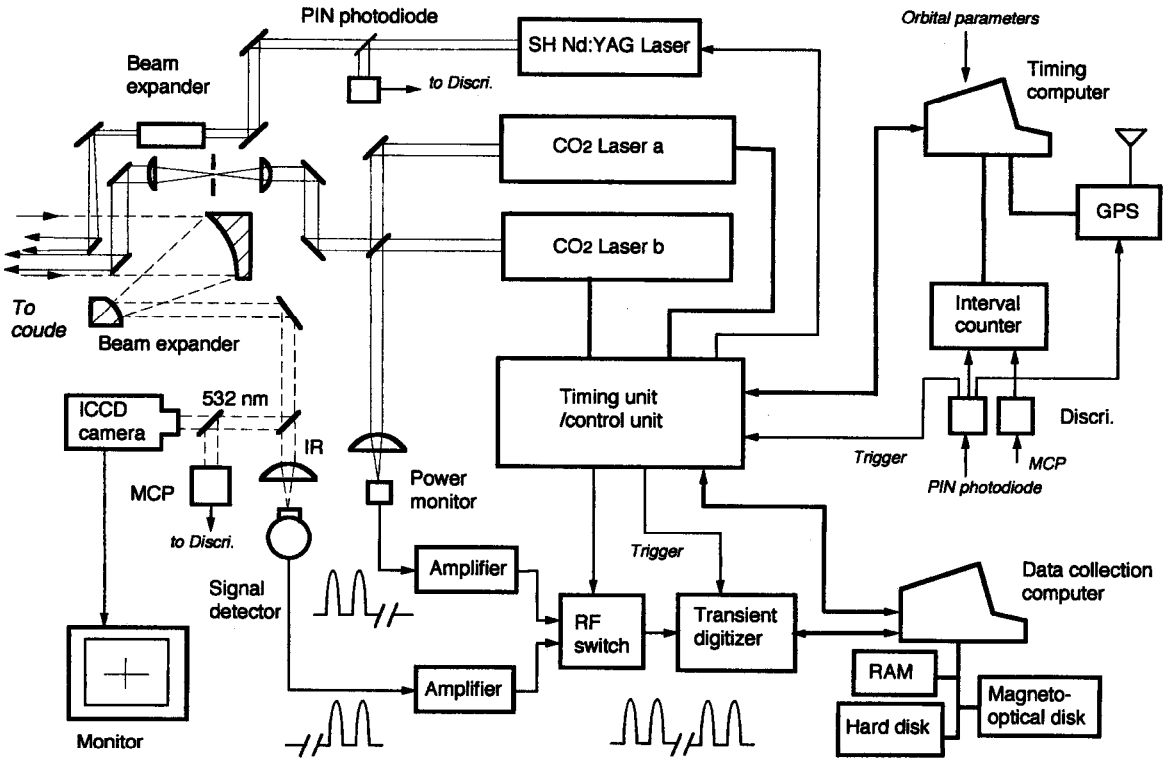

Figure 6. Block diagram of the laser transmitter/receiver system.

Figure 6 shows a detailed schematic diagram of the laser transmitter/receiver system. The beams from the two lasers were collimated and combined with a half mirror. The combined beam was directed to the Coude path of the 1.5 m telescope and transmitted to the RIS. The repetition rate of the TEA lasers was 50 Hz, and the time interval between pulses from two lasers was 200 μs. The transmitted pulse energy was typically 50 mJ at 10 μm. The reflected signal from the RIS was collected with the same telescope and focused on a HgCdTe detector cooled at 77 K. A portion of the transmitted beam was picked off and directed to a room temperature HdCdTe detector to monitor the power. The waveforms of transmitted and received laser pulses were recorded at every shot with a high-speed transient digitizer. The time gate for recording the received pulse was predicted using the orbital parameters for the ADEOS satellite. Table 1 lists the parameters of the ground system (Ozawa *et al* 1997b).

3. Optical characteristics of the RIS in orbit

Active tracking of the RIS was established using the image taken with the intensified charge coupled device (ICCD) cameras on the guide telescope and in the Coude system of the main telescope. The image of the RIS at 532 nm lit by the second harmonics Nd:YAG laser was clearly observed both in the daytime and night-time. The background noise in the daytime measurement was reduced to a negligible level by applying a gate to the ICCDs with a duration of 10 μs. Interference filters with a bandwidth of 10 nm were also used to reduce the background noise. Accuracy of tracking was evaluated from the fluctuation of the recorded ICCD images, and it was better than 30 μrad.

To confirm the optical characteristics of the RIS in orbit, we evaluated the efficiency of the reflection first at 532 nm. We measured the efficiency by comparing the image of the RIS with the images of stars. The efficiency, η (m^{-2}), is defined so that the received power is calculated by the following equation:

$$P = (16/\pi^2)(P_0/\theta_t^2)T^2\eta_{\mathrm{RIS}}A_r\eta_{\mathrm{sys}}\eta, \qquad (2)$$

where $P_0, \theta_t, T, \eta_{\mathrm{RIS}}A_r$, and η_{sys} represent transmitted power, divergence of the transmitted beam, transmittance of the atmosphere, reflectance of the RIS, aperture of receiver, and optical efficiency of the receiver system, respectively.

In the measurement, the beam from the Nd:YAG laser at 532 nm was diverged in the Coude path and transmitted from the 1.5 m primary mirror with a beam divergence of 0.5 mrad. Transmitted laser energy was 30 mJ/pulse. The reflection from the RIS was observed with the ICCD camera on the guiding telescope with a diameter of 20 cm. The observed image was recorded with a video recorder, and the intensity of the return was estimated from the recorded image.

We first measured images of stars with different stellar magnitudes to confirm the reproducibility of the intensity measurement. We also considered the difference in the intensity measurements of the continuous and pulsed light sources. Since the repetition rate of the Nd:YAG laser was 10 Hz, and the integration time of the ICCD camera was $\frac{1}{30}$ s, we multiplied $\frac{1}{3}$ to the intensity of the image of the RIS

Table 1. Ground system parameters.

TEA CO_2 Laser for spectrum measurement	
Output pulse energy	100 mJ (10 μm)
Pulse repetition	50 Hz
Line frequency stability	<10 MHz
Transmitted beam divergence	0.09 mrad
SH Nd:YAG laser for satellite tracking and ranging	
Output pulse energy	30 mJ (532 nm)
Pulse repetition	10 Hz
Transmitted beam divergence	0.5 mrad
Receiver telescope	
Diameter	1.5 m
Guide telescope diameter	0.2 m
Detector	
Detectivity	7×10^{10} cm $Hz^{1/2}$ W^{-1} (10 μm)
Area	0.001 cm^2
Quantum efficiency	0.6
Transient digitizer	
Sampling rate	100 MHz (maximum)
Accuracy	8 bits

recorded in a frame to avoid overestimating. The return from the RIS measured with the ICCD camera was comparable to a stellar magnitude of 2–4 depending on the elevation angle. We derived the efficiency of the reflection from the RIS using equation (2). We assumed that $T = 0.7$ and $\eta_{RIS} = 0.8$. The response of the detection system, including the optical efficiency of the receiver system, was calibrated with the intensities of stars.

Figure 7(*a*) shows the measured efficiencies of the reflection from the RIS for different night-time paths (Ozawa *et al* 1997a). The maximum elevation angle is higher in the upper path shown in the figure. The horizontal axis indicates the time that corresponds to the location of the ADEOS along the path. The elevation angle to the ADEOS reached its maximum at the end of the measurement. The theoretical efficiencies for the same paths are shown in figure 7(*b*) which were calculated based on the wavefront of the RIS PFM. In the calculation, the ground pattern, such as shown in figure 3, was calculated for each location of the RIS along the path, and the received power was estimated based on the ground system parameters. The efficiency defined by equation (2) was then calculated (Sugimoto *et al* 1996). The measured and theoretical efficiencies are compared for daytime paths in figures 8(*a*) and (*b*). The measured efficiency was affected by atmospheric conditions and tracking errors. Also, there were occasional delays in the initial capture of the RIS. However, the maximum efficiency for each path agreed well with the theory. We consequently concluded that the RIS was working well in orbit.

We evaluated the intensity of the infrared reflection from the RIS by comparing the return signal with that from a 3 cm diameter hollow retroreflector installed on a tower located 4.2 km from the ground station. Figure 9 shows an example of the waveforms of a pair of transmitted and received CO_2 laser pulses in the measurement with the RIS. It can be seen in the figure that the signal-to-noise ratio (SNR) of the detection of the returns was fairly high. The result of the comparison with the tower retroreflector showed that the signal intensity from the RIS at maximum was comparable to that from the tower retroreflector when an optical attenuator of 10^{-5} was used with a 100 times smaller detector gain.

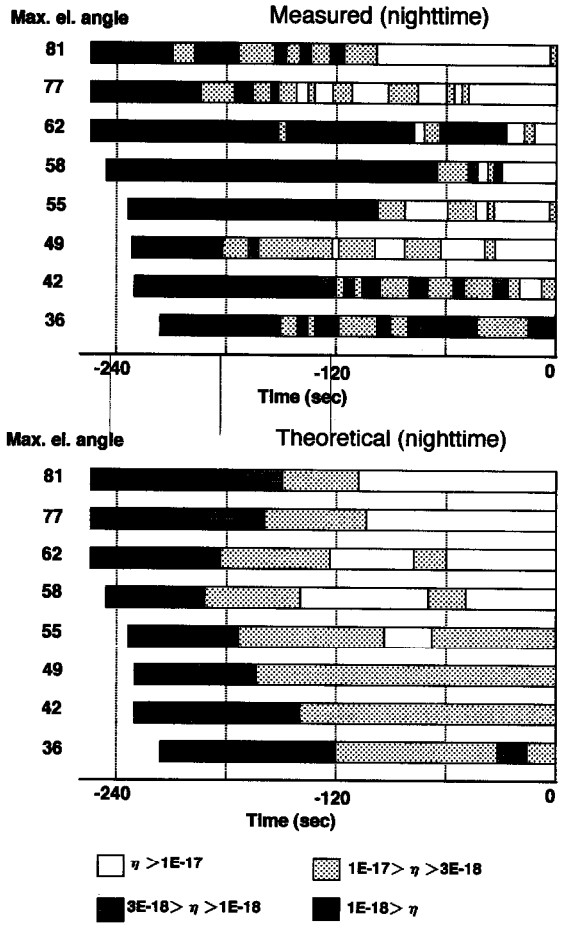

Figure 7. Measured (upper) and theoretical (lower) efficiency of reflection of the RIS for night-time paths.

The transmitted beam divergence for the RIS and the tower reflector was 9.0×10^{-5} rad and 2.5×10^{-5} rad, respectively, and the assumed atmospheric transmittance was 0.9 for the RIS and 0.97 for the tower. The efficiency, η, for the tower

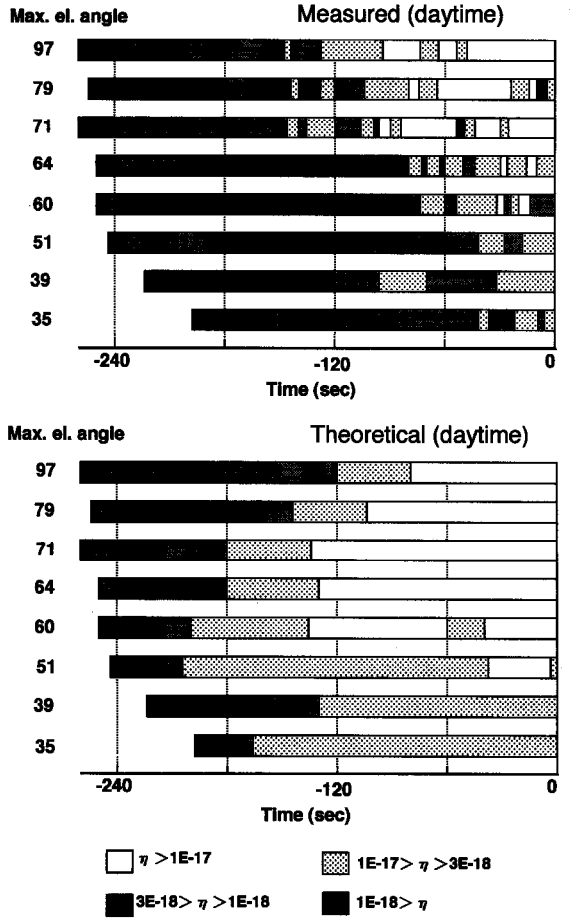

Figure 8. Measured (upper) and theoretical (lower) efficiency of reflection of the RIS for daytime paths.

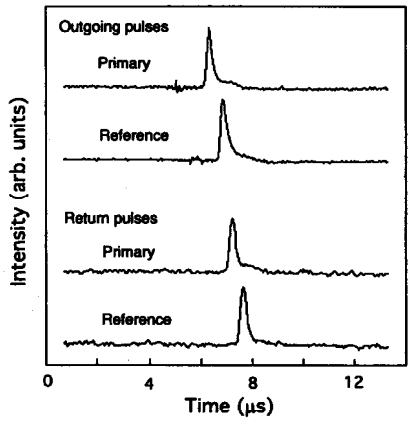

Figure 9. Example of the recorded waveforms of a pair of transmitted and received CO_2 laser pulses in the measurement with the RIS at 10 μm.

retroreflector was 2.2×10^{-11} m^{-2}. Using these parameters, the efficiency for the RIS at 10 μm was estimated to be 3.3×10^{-17}. It agreed well with the designed value 4×10^{-17} (Ozawa *et al* 1997b). We did not apply this method to the evaluation of the visible efficiency because a higher accuracy was expected with the method using stars.

4. Laser long-path absorption experiment and error analysis

4.1. Spectroscopic experiment

We carried out the experiments on the spectroscopic measurement of ozone using the TEA CO_2 lasers. As mentioned earlier, we planned the measurement of ozone, CFC12, HNO_3 with the fundamental of the CO_2 lasers, CO and N_2O with the second harmonics, and CH_4 with the third harmonics. We began the experiment with ozone, because ozone was the most suitable target for validating the measurement technique in comparison with other techniques. We performed a simultaneous measurement with a laser heterodyne spectrometer (Fukunishi *et al* 1990) at the same location to validate the measurement with the RIS.

In the measurement of ozone, the two TEA CO_2 lasers were tuned to a $9P(24)$ line of $^{12}CO_2$ and a $10R(24)$ line of $^{13}CO_2$ as on-line (primary) and off-line (reference) wavelengths, respectively. Figure 10 shows the measured spectrum data with the RIS. The vertical axis indicates the logarithm of the ratio of the signal intensity for primary laser to that for reference laser. The horizontal axis indicates the shot number. Since the magnitude of the Doppler shift of the return light changes with time, the wavelength of the return light changes with the shot number. The repetition rate of the lasers was 50 Hz, and 10 000 pulse pairs were recorded in the measurement.

Figure 11 shows the theoretical absorption spectrum which was calculated for the one-way path from the ground to the top of the atmosphere based on the HITRAN96 database for atmospheric absorption lines. The US Standard Atmosphere was used for the molecular vertical distributions. The continuum absorptions of water vapour and aerosols are not included in this figure. The spectral ranges covered with the Doppler shift are indicated in the figure. Around the $9P(24)$ line of $^{12}CO_2$ laser, there is a sharp absorption line of ozone on the shoulder of a broad absorption line of atmospheric CO_2. On the other hand, absorption is small at the $10R(24)$ line of a $^{13}CO_2$ laser. Figure 12 shows simulated signals for the RIS measurement which were calculated based on the theoretical spectrum shown in figure 11 and the simulated efficiency of the reflection of the RIS. It can be seen that the dip seen in the measured spectrum is due to the absorption of ozone that the $9P(24)$ line of $^{12}CO_2$ laser receives. The shape of the absorption in the measured spectrum is not symmetrical because both the path length and the wavelength change in the measurement.

We derived column contents of ozone from the measured spectrum by fitting the theoretical spectrum by means of the least-squares method. The contributions of the water vapour continuum absorption and the difference in optical efficiency of the system at the two wavelengths were determined at the same time with ozone column contents in the least-squares fitting. The US Standard Atmosphere was used for the vertical distribution of CO_2. We obtained the column contents of ozone of 8.6×10^{18} cm^{-2}. The column contents obtained with the simultaneous heterodyne spectrometer

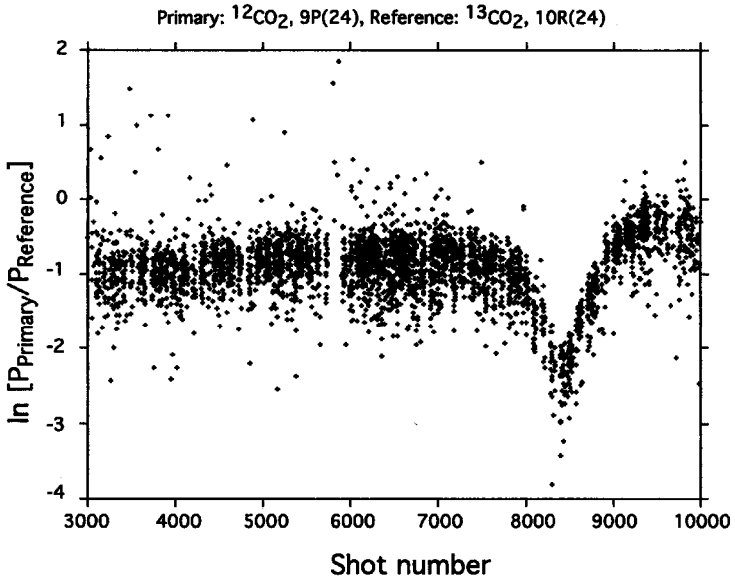

Figure 10. Spectrum measured with the RIS.

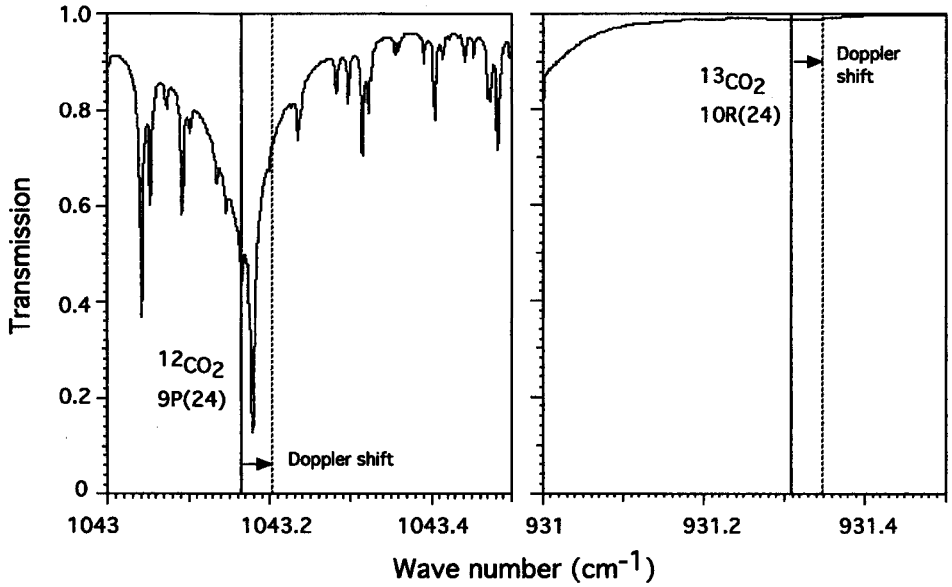

Figure 11. Theoretical absorption spectrum around the laser wavelengths.

measurement were $8.3 \times 10^{18} cm^{-2}$ and agreed well with the RIS measurement.

An inversion method can be applied to derive vertical profile of ozone, if the SNR of the measured spectrum is sufficiently high. However, the SNR of the spectrum shown in figure 10 is insufficient to derive the vertical profile. We carried out several measurements in the same spectral region and the results were similar. Although the intensity of the return signals agreed well with the theory as described earlier, the fluctuation of the signals was larger than expected. The fluctuation was not completely cancelled in the ratio of signals of primary and reference wavelengths. We investigated the error in the measurement to identify the cause of the error and to improved the measurement system.

4.2. Analysis of measurement error

We analysed measurement error in the data taken with the RIS to evaluate the measurement method. There are various causes of noise in the received signals. They are: detector noise, digitization noise of an analogue to digital converter, atmospheric turbulence, fluctuation of laser beam pattern, satellite tracking error, etc. Among them, the noises caused by atmospheric turbulence, beam fluctuation, and satellite tracking error are proportional to the recorded signal

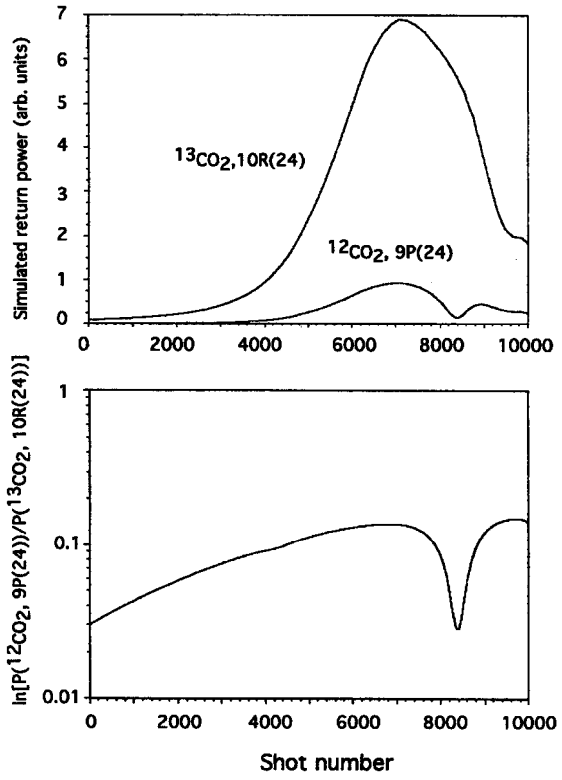

Figure 12. Simulated signals for the RIS measurement.

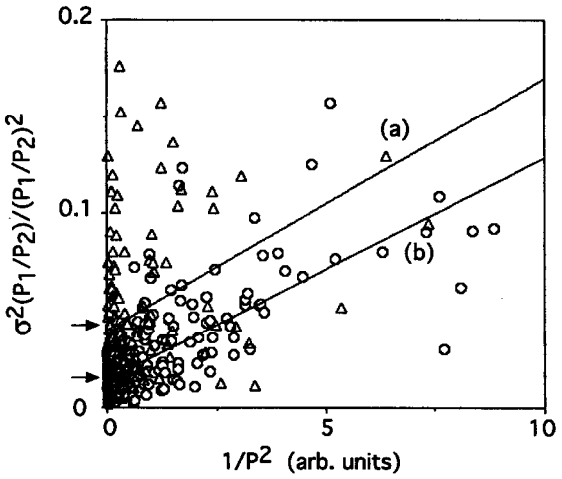

Figure 13. The square of error in (P_{pri}/P_{ref}) as a function of the square of $(1/P_{ref})$.

intensity. On the other hand, detector noise and digitization noise are independent of the signal intensity. To identify the dominant cause of the measurement error, we analysed the dependence of the error on the signal intensity.

Figure 13 shows the square of the standard deviation of (P_{pri}/P_{ref}) as a function of the square of $(1/P_{ref})$. Both primary and reference lasers were tuned to $10P(24)$ of $^{12}CO_2$. The normalized squared standard deviation of (P_{pri}/P_{ref}) can be written as

$$\langle\Delta(P_1/P_2)^2\rangle/(P_1/P_2)^2 = \langle\Delta P_1\rangle^2/P_1^2 + \langle P_2\rangle^2/P_2^2 - 2\langle\Delta P_1\Delta P_2\rangle/(P_1P_2), \quad (3)$$

where P_1, P_2 represent the averaged received power for primary and reference lasers, and ΔP_1, ΔP_2 their deviations. The third term in equation (3) represents covariance. If ΔP_1 and ΔP_2 are correlated, the third term cancels the first and the second terms in equation (3). In the actual signals, there are correlated and non-correlated components.

The standard deviation of the received power for each laser can be written as

$$\langle\Delta P^2\rangle = A + BP^2, \quad (4)$$

where the first term represents the noise independent of the signal intensity. The second term represents the noise proportional to the signal intensity. We may write the dependence of $\langle\Delta(P_1/P_2)^2\rangle/(P_1/P_2)^2$ on the signal intensity in the same way:

$$\langle\Delta(P_1/P_2)^2\rangle/(P_1/P_2)^2 = A'/P^2 + B', \quad (5)$$

where we have assumed $P_1 = P_2 = P$. The first term represents the contribution of the noises in the received signal which is independent of the signal intensity, and the second term represents the contribution of the noise proportional to the signal intensity. In figure 13, $\langle\Delta(P_1/P_2)^2\rangle/(P_1/P_2)^2$ is plotted as a function of $1/P^2$. The slope of the plot, consequently, indicates the contribution of the detection noise independent of the received signal intensity, and the constant indicates the noise proportional to the signal intensity.

Figure 13(*a*) shows data taken with the RIS before improvement of the transmitter system. We calculated the standard deviation for the data sets consisting of ten successive pulse pairs. The second term in equation (5) is large in this case, and it can be concluded that the contribution of the noise proportional to the signal intensity is dominant. We found that the largest cause of the noise was the difference in the transmitted beams from the two CO_2 lasers, though both lasers had a TEM00 transverse mode. To improve the transmitted beam pattern, we added a spatial filter which consisted of a pair of lenses, a pinhole, and apertures to the transmitter optics after combining the beams from the primary and reference lasers. Figure 13(*b*) shows the result after the improvement of the transmitter. The noise proportional to signal intensity was reduced. As to the noise independent of received signal, we cannot compare the two cases in figure 13, because P in the figure is in a relative scale.

We also studied the power spectrum of shot-to-shot variation of the received signal intensity and the ratio of the signals for the two lasers. We used the Lomb method (Lomb 1976) to derive a power spectrum instead of the regular fast Fourier transformation because data points were sometimes missing. Figure 14 shows the results. The upper panel shows the power spectrum of the signal intensity, and the lower panel shows the ratio of the signals. Trace (*a*) indicates the data taken before the improvement of the system, and trace (*b*) shows the data after the improvement using the spatial filter. Trace (*c*) shows the data after further improvement on

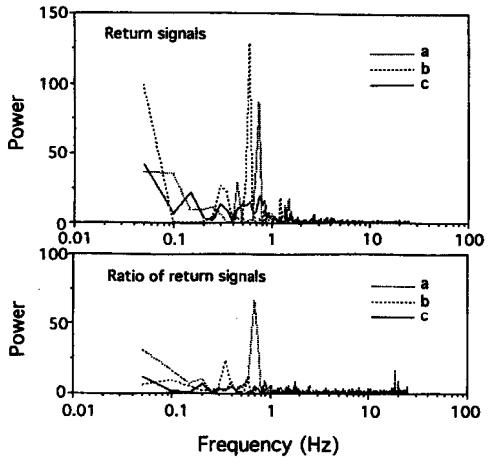

Figure 14. Power spectrum of shot-to-shot variation of the signal intensity (upper) and the ratio of the signals for the two lasers (lower).

the satellite tracking system. The noise component having a frequency around 0.6–0.8 Hz is the satellite tracking error. This noise component is also seen in the ratio of the signals in trace (*a*), but it is improved in trace (*b*). This shows that the difference of the beam pattern of the two lasers was the cause of the noise before using the spatial filter. After the improvement of the satellite tracking system, the noise component is small even in the power spectrum of the signal intensity. In all cases in figure 14, noise with a higher frequency component which may be caused by interference in a retroreflector array is not seen. This shows the feature of the RIS having a single element structure.

The SNR obtained with the improved system was approximately ten in the ratio of the received signal for the single pulse pair. It corresponds to the error of approximately 2% in the column contents of ozone.

5. Conclusion

We demonstrated the Earth–satellite–Earth laser long-path absorption method for measuring atmospheric trace species for the first time using the RIS. We measured the absorption spectrum of atmospheric ozone using the Doppler shift method and obtained column contents. We validated the measurement with a simultaneous heterodyne spectrometer measurement. Because of the unexpected discontinuance of the ADEOS operation, we were not able to implement experiments on the measurement of other species, as originally planned. However, we were able to evaluate the measurement technique.

We also demonstrated the new design hollow cube-corner retroreflector with a curved mirror surface. Since a single element retroreflector is free from interference between elements, it is ideal for laser long-path absorption measurements and also for accurate satellite laser ranging. Though a single element retroreflector has a small active angler area, we may use four elements to cover a half-sphere with a small interference between elements (Minato and Sugimoto 1998). Such a retroreflector design will be useful for accurate satellite laser ranging.

Based on the results obtained with the RIS, we are studying the Earth–satellite laser long-path absorption system using a geostationary satellite (Sugimoto 1987, Sugimoto 1995c). In this technique, the laser beam is received with a detection system on the geostationary satellite instead of reflecting with a retroreflector. With this method, we can continuously perform measurements from the multiple ground station. Theoretical study shows that important atmospheric trace species, such as CO_2, O_3, CH_4, N_2O, CO, NO, NO_2, HNO_3, HCl, HF, NH_3, OCS, C_2H_6, C_2H_2, H_2CO, can be measured with this method in the infrared region. This technique does not require large receiving telescopes and large laser power at ground stations. However, continuously tunable narrow-band infrared pulsed lasers are required because the Doppler shift method cannot be applied to the measurement with a geostationary satellite. We are studying the feasibility of this technique.

Acknowledgments

This work was funded by the Global Environment Research Fund of the Environment Agency of Japan. The RIS experiment was conducted in the ADEOS program of the National Space Development Agency of Japan. The authors also wish to thank all the satellite laser ranging stations that participated in the laser ranging support to the RIS experiment.

References

Fukunishi H, Okano S, Taguchi M and Ohnuma T 1990 *Appl. Opt.* **29** 2722–8
Hinkley E D (ed) 1976 *Laser Monitoring of the Atmosphere* (Berlin: Springer) ch 6
Lomb N R 1976 *Astro. Space Sci.* **39** 447–62
Minato A and Sugimoto N 1998 *Appl. Opt.* **37** 438–42
Minato A, Sugimoto N, Bleier Z, Hunter G C and Paul J 1995 *Opt. Rev.* **2** 319–22
Minato A, Sugimoto N and Sasano Y 1992 *Appl. Opt.* **31** 6015–20
Nordstrom R J, Berg L J, DeSimone A F and Sugimoto N 1993 *Rev. Sci. Instrum.* **64** 1663–4
——1994 *Rev. Laser Eng.* **22** 132–9
Ozawa K, Koga N, Sugimoto N, Saito Y, Nomura A, Aoki T, Itabe T and Kunimori H 1997b *Opt. Eng.* **36** 3235–41
Ozawa K, Sugimoto N, Koga N, Kubota Y, Saito Y, Nomura A, Minato A, Aoki T, Itabe T and Kunimori H 1997a *Opt. Rev.* **4** 450–2
Sugimoto N 1987 *Appl. Opt.* **26** 763–4
Sugimoto N and Minato A 1994 *Opt. Eng.* **33** 1187–92
——1995b *IEICE Trans. Common.* E **78** 1585–90
——1996 *Opt. Rev.* **3** 62–4
Sugimoto N, Minato A, Matsui I, Sasano Y, Itabe T, Aoki T, Takabe M, Hiromoto N and Kunimori H 1995a *SPIE* **2583** 217–27
Sugimoto N, Minato A, Ozawa K, Saito Y and Nomura A 1995c *Japan. J. Appl. Phys.* **34** 2329–34
Sugimoto N, Minato A and Sasano Y 1991 *Conf. Lasers and Electro-Optics Technical Digest Series (Washington, DC, 1991)* vol 10, p 450